Water Dipole and Quadrupole Moment Contributions to the Ion Hydration Free Energy by the Deep Neural Network trained with Ab Initio Molecular Dynamics Data

Yu Shi, Carrie C. Doyle, Thomas L. Beck*

Department of Chemistry, University of Cincinnati, Cincinnati, Ohio 45221, United States

E-mail: shiy4@ucmail.uc.edu

Abstract

We report a calculation scheme on water molecular dipole and quadrupole moments in the liquid phase through a Deep Neural Network (DNN) model. Employing the the Maximally Localized Wannier Functions (MLWF) for the valence electrons, we obtain the water moments through a post-process on trajectories from *ab-initio* molecular dynamics (AIMD) simulations at the density functional theory (DFT) level. In the framework of the deep potential molecular dynamics (DPMD), we develop a scheme to train a DNN with the AIMD moments data. Applying the model, we calculate the contributions from water dipole and quadrupole moments to the electrostatic potential at the center of a cavity of radius 4.1 Å as -3.87 V, referenced to the average potential in the bulk-like liquid region. To unravel the ion-independent water effective local potential contribution to the ion hydration free energy, we estimate the 3rd cumulant term as -0.22 V from simulations totally over 6 ns, a time-scale inaccessible for AIMD calculations.

Introduction

The hydration free energy is of vital importance for understanding single-ion solvation in aqueous solution. While there is no direct way to measure the single-ion hydration free energy, extra-thermodynamic assumptions are introduced, as summarised in works by Beck and Pollard,[1–3] to estimate single-ion value from ion-pair hydration data in the bulk liquid phase. For example, assuming that the enthalpy difference is a linear function of the inverse of the cube of effective ion radius in the large-ion limit[4] , Marcus reported the proton hydration free energy -254.3 kcal/mol;[5] Ashbaugh and Asthagiri[6] revisited the Born-like hydration free energy assumption in the LPS method[7] and gave the proton hydration free energy scale close to that reported in Marcus's work. Alternatively, by combining the ion-pair bulk values with single-ion small cluster (number of water n$\leq$ 6) hydration data, the cluster-pair approximation (CPA)[8] gives proton hydration free energy -265.9 kcal/mol, which has been revised recently by Beck as -264.7 kcal/mol. In addition, for Na^+ ion, Marcus gave -91.5 kcal/mol, CPA gave -101.3 kcal/mol. Clearly, there is a free-energy shift of the order of -10 kcal/mol (-0.40 eV) from the bulk ion-pair data estimation. Beck showed that,[1,2] the shift arises from the large-cluster limit in CPA where there are two interface potential shifts, one is the vapor-water interface potential (surface potential ϕ_{sp}) and the other one is the water-solute interface potential (local potential ϕ_{lp}). The interface potential shift of cation cancels out that of anion, resulting in the absence of interface potential contributions from the ion-pair bulk hydration data in the Marcus's work.[5] Calculations[2] with polarizable water-model indicate that the net potential ($\phi_{np} = \phi_{sp} + \phi_{lp}$) is between -0.40 V and -0.50 V and it is independent of identity of the solvated ion. Considering that the surface potential ϕ_{sp} is a liquid water property around 3.5 V,[9,10] it suggests that local potential should be a liquid water property, too. Partitioning the hydration free energy with the quasi-chemical theory perspectives[11] shows that the ϕ_{lp} comes into the hydration free energy from the interaction energy of solute ion with water molecules outside a cavity. Simulations with SPC/E water model yields a local potential 0.42 V (9.7 kcal/mol·e)[12] for a cavity of radius 6.15 Å . The

SPC/E water model generates the surface potential -0.6 V (-13.8 kcal/mol·e),[13,14] leaving the net potential ϕ_{np} = -0.18 V. Note that the ϕ_{lp} is regarded as an effective potential, it is the summation of the first and the third terms (0.35 V + 0.07 V , the linear charge-dependent terms, see the detailed discussion in next section) of the cumulant expansion for hydration free energy calculation.

The *ab initio* multipole analysis in the work by Mundy[15] gives the dipole contribution to the surface potential 0.48 V, the Bethe potential 3.84 V and thus ϕ_{sp} = 4.32 V. The large difference of surface potential between classical MD and AIMD arises from that the classical charge distributions are approximated as partial charges on each charging sites. While the partial charge model is very computationally efficient, they fail to accurately represent the electron density. Stitching the profile of average potential in the vapor surface vicinity together with the potential profile in the vicinity of a cavity of radius 4 Å , they estimated ϕ_{np} = 0.08 V, and thus ϕ_{lp} = -0.40 V. However this should be regarded as the contribution from the first cumulant term.

In the present work, following the previous works,[16–18] we use the MLWF to calculate the dipole and quadrupole moments for each water molecule in each configuration of an AIMD simulation trajectory. Then we calculate the moment contributions to the potential at the center of a cavity of radius 4.1Å . As mentioned above, we should approach the third cumulant term, which is inaccessible to the AIMD simulations considering that the classical MD with SPC/E water approached a convergent estimate over 4 ns.[12] Recent advances in neutral network potentials (NNP) have created a new category of simulation protocols where quantum accuracy can be achieved at the low cost of classical MD. Neural networks are one of the most advanced techniques used to develop machine learning (ML) potentials. These potentials must satisfy criteria of: (1) the analytic structure-energy relationship is expressed using a ML, (2) they must use a first-principles training set of energies and forces (3) they cannot containing any *ad hoc* assumptions.[19] The general steps to construct a neural network potential (NNP) are as follows. First, an initial set of electronic structure

calculations is generated. This is often the most computationally expensive element which establishes the bottleneck. Next, the data needs to be transformed into appropriate input features that satisfy conditions of both rotation and translation invariant system energy and permutation symmetry with the exchange symmetry of like atoms. Parameters are then varied to agree with the training data energies and forces in order to construction of Potential Energy Surface (PES). Finally the model is tested and simulations follow. One such NNP is the DPMD potential of Car and coworkers that has been shown to accurately represent the PES[19–22] and produce accurate simulation of condensed phase systems.[23,24] In the context of the electrostatics of molecular liquids, the NNP approach is a new way to access the time scales of interest without sacrificing the accuracy of electron density. Here, we calculate the dipole and quadrupole moments of liquid water and the local potential ϕ_{lp} at the cavity center. First we give explicit expression of the local potential contribution to the hydration free energy; Second we describe the workflow of our procedure, utilizing the original DPMD-kit of Zhang et al,[25] as well as a slightly edited version. Finally we present and discuss results of our calculations.

Theoretical Methodology

The excess chemical potential for an ion X is given by the Widom formula[11]

$$\mu_X^{ex} = -kT \ln \langle e^{-\varepsilon_X/kT} \rangle_0 \tag{1}$$

where ε_X is the interaction energy of the ion with the solvent and the zero subscript indicates the ion and waters are of no interaction. The textbook expression for the electrochemical potential[26,27] for an ion X is

$$\mu_X^{ex} = \mu_{X,bulk}^{ex} + q_X \phi_{np} \tag{2}$$

where $\mu_{X,bulk}^{ex}$ is the free energy deep in the liquid phase. We employed the quasichemical theory (QCT)[11] to compute the hydration free energy of the Na$^+$ ion. QCT partitions the free energy spatially into three physical parts. The hydration free energy can then be expressed as[12]

$$\mu_X^{ex} = -kT \ln \langle e^{-M_\lambda/kT} \rangle_0 - kT \ln \langle e^{-\varepsilon_X/kT} \rangle_{M_\lambda + \varepsilon_X} + kT \ln \langle e^{-M_\lambda/kT} \rangle_{\varepsilon_X} \qquad (3)$$

where M_λ is the cavity potential, and the first term (packing) is the free energy change to grow a cavity of radius λ in the liquid, the second term (long-ranged) is the free energy change for inserting the ion into the cavity center and the last term (inner-shell) is minus the free energy change to grow the same cavity in the liquid around an ion. The interfacial potential contribution to the free energy resides in the long-ranged term, for which the cumulant expansion is

$$\mu_{X,LR}^{ex} = -kT \ln \langle e^{-\varepsilon_X/kT} \rangle_{M_\lambda} = \langle \varepsilon_X \rangle_{M_\lambda} - \frac{1}{2kT} \langle \delta \varepsilon_X^2 \rangle_{M_\lambda} + \frac{1}{6(kT)^2} \langle \delta \varepsilon_X^3 \rangle_{M_\lambda} \qquad (4)$$

$$\varepsilon_X = q\phi + \varepsilon_{ind} + \varepsilon_{disp} \qquad (5)$$

where ϕ is the cavity potential from the unperturbed molecular charge distributions, ε_{ind} is the ion-induced-dipole induction interaction, ε_{disp} is the ion-water dispersion interaction. The induction energy is proportional to the q^2 and thus is ignored. In a recent work where there is Na$^+$ ion at the center, the dispersion interactions is -0.02 kcal/mol. Therefore it is plausible to neglect the dispersion interaction energy and only consider the dominant electrostatic interaction for the higher cumulant terms,

$$\mu_{X,LR(es)}^{ex} = q\langle \phi \rangle_{M_\lambda} - \frac{q^2}{2kT} \langle \delta \phi^2 \rangle_{M_\lambda} + \frac{q^3}{6(kT)^2} \langle \delta \phi^3 \rangle_{M_\lambda} \qquad (6)$$

and the effective local potential is given as

$$\phi_{lp} = \langle \phi \rangle_{M_\lambda} + \frac{q^2}{6(kT)^2} \langle \delta\phi^3 \rangle_{M_\lambda} \tag{7}$$

the first term $\langle \phi \rangle_{M_\lambda}$ is the electrostatic potential at the center of a cavity of radius λ, and $\delta\phi$ is the fluctuation of the center potential. In simulations where electrostatic interactions are evaluated using Ewald summation with conducting boundary conditions, the average potential of the bulk liquid phase is referenced as zero.[28] In the present work, we employ this reference for our potential calculations. In the previous works[13,29] the center potential $\langle \phi \rangle_\lambda$ is defined as

$$\langle \phi \rangle_{M_\lambda} = (-1) \left[\delta\phi_r^D(r) + \delta\phi_r^{Q,1}(r) + \delta\phi_r^{Q,2}(r) \right] \tag{8}$$

The dipole moment contribution to the center potential $\delta\phi_r^D$ is determined from the dipole moment density $P_r(r)$

$$\delta\phi_r^D(r) = \frac{1}{4\pi\epsilon_0} \int_0^r \frac{4\pi r'^2 P_r(r')}{r'^2} dr' \tag{9}$$

the quadrupole moment contribution to the center potential $\delta\phi_r^{Q,1}(r)$ is accessible from the simulation data via the radial dependence of the quadrupole moment density written in spherical coordinates, $Q^s(r)$

$$\delta\phi_r^{Q,1}(r) = -\frac{1}{4\pi\epsilon_0} \frac{4\pi r^2 Q_{rr}^s(r)}{r^2} \tag{10}$$

where the radial element is $Q_{rr}^s(r)$. The second quadrupole contribution is from the broken-symmetry of the quadrupole diagonal elements of waters in the vicinity of the cavity interface,

$$\delta\phi_r^{Q,2}(r) = \frac{1}{4\pi\epsilon_0} \int_0^r \frac{4\pi r'^2 [TrQ(r') - 3Q_{rr}^s(r')]}{r'^3} dr' \tag{11}$$

Computational Methodology

In the following section we discuss the methodology on how to calculate the water molecular dipole and primitive quadrupole moments in liquid phase at the quantum accuracy through simulations over timescale of nano-seconds.

AIMD Simulation Setup

Both neat-water system and cavity-water system consist of 64 water molecules. The size of each simulation cubic box is $L = 12.4295$ Å and $L = 13.0236$ Å. The cavity potential $M_{\lambda=4.10}(r)$ is a harmonic potential

$$M_{4.1}(r) = k(r - 1.05\lambda)^2 \tag{12}$$

where k = 40 kcal/mol/Å². With the QuickStep module in the CP2K 2.6.1 package, for the two systems we performed DFT simulations by employing the Gaussian-type basis sets (DZVP-MOLOPT-SR-GTH) and the Goedecker-Teter-Hutter (GTH) pseudo-potentials. We use the functional revised Perdew,Burke and Ernzerhof (revPBE), together with a dispersion correction, Grimme D3 and set up the plane waves cutoff at 400 Ry. We apply the Nosé-Hoover thermostat chain of length 3 to maintain a temperature 330 K. We treat electrostatic interaction under the periodic boundary with Ewald method. Both simulations run for 30 ps with a time step 0.5 fs in the NVT ensemble, generating 60,000 configurations along with the total potential energy E, force on each atom $\mathbf{F_i}$.

We regard water molecule as a neutral entity and use following expressions from previous work[17] to calculate the dipole moment $\mathbf{P}$ by

$$\mathbf{P} = \int_{cell} d\mathbf{r}\rho_e(r)(-2)\mathbf{r} + \sum_i Z_i\mathbf{R_i} \tag{13}$$

where $\rho_e(\mathrm{r})$ is the valence electron density function, Z_i is the ith atom charge, R_i is the ith

atom position. The primitive quadrupole moments $Q_{\mu\nu}$ is given by

$$Q_{\mu\nu} = \frac{1}{2}\int_{cell} d\mathbf{r}\rho_e(r)(-2)(r_\mu r_\nu) + \frac{1}{2}\sum_i Z_i R_{i,\mu} R_{i,\nu} \tag{14}$$

and the traceless quadrupole moment by

$$Q'_{\mu\nu} = \frac{1}{2}\int_{cell} d\mathbf{r}\rho_e(r)(-2)(3r_\mu r_\nu - \delta_{\mu\nu}r^2) + \frac{1}{2}\sum_i Z_i(3R_{i,\mu}R_{i,\nu} - \delta_{\mu\nu}R_i^2) \tag{15}$$

Both $\mathbf{R_i}$ and $\mathbf{r}$ are referenced to the oxygen atom. We use the CRAZY method in the CP2K package to get MLWF with a convergence of 10^{-8} , and then Wannier center of the nth MLWF r_n is given as

$$\langle r_{n,\mu}\rangle = \frac{L}{2\pi}\Im(\ln\langle\phi_n|e^{i\frac{2\pi}{L}r_\mu}|\phi_n\rangle) \tag{16}$$

and the electron quadrupole moment elements are given as

$$\langle r_\mu r_\nu\rangle_n = \langle r_\mu\rangle_n\langle r_\nu\rangle_n + \frac{L^2}{16\pi^2}\{\ln|\langle\phi_n|e^{i\frac{2\pi}{L}r_\mu}e^{-i\frac{2\pi}{L}r_{nu}}|\phi_n\rangle|^2 - \ln|\langle\phi_n^{i\frac{2\pi}{L}r_\mu}e^{i\frac{2\pi}{L}r_\nu}|\phi_n\rangle|^2\} \tag{17}$$

and if R_o is the oxygen position, then we get the elements with respective oxygen as

$$\langle r_\mu^o r_\nu^o\rangle_n = \langle r_\mu r_\nu\rangle_n - R_{o,\mu}\langle r_\nu\rangle_n - R_{o,\nu}\langle r_\mu\rangle_n + R_{o,\mu}R_{o,\nu} \tag{18}$$

DNN Setup for Potential Energy Surface and Multipole Moments

In the DPMD framework, a local coordinate frame should be constructed to preserve transition and rotation symmetry. Permutational symmetry is preserved though ordering neighboring atoms by their species first and then in order of increasing inverse distance from the atom of interest. We set up the local coordinate system $(\mathbf{e_x}, \mathbf{e_y}, \mathbf{e_z})$ following the protocol in the previous works[21,22] that $\mathbf{e_x}$ is along the O-H bond, where the atom H is the closest to the oxygen atom; $\mathbf{e_z}$ is perpendicular to the plane of the water molecule; $\mathbf{e_y} = \mathbf{e_z} \times \mathbf{e_x}$.

Within the local coordinate system, the descriptors are assembled for each atom, including the full radial and angular information for the 24 oxygen atoms and 48 hydrogen atoms (the number of neighboring oxygen in the hydration first shell of oxygen atom) and only radial information for 36 oxygen atoms and 72 hydrogen atoms within $R_c = 6$Å. As the first layer, the descriptors of each atoms flow into a DNN of 5 hidden layers with decreasing number of neurons as $(240, 120, 60, 30, 10)$, which maps descriptor into the atomic energy E_i as the output. The non-linear activation function is taken to be the hyperbolic tangent, and forces on each atom is computed as negative derivative with respect to its position. The loss function is

$$L(p_\epsilon, p_f) = \frac{p_\epsilon}{N}\Delta E^2 + \frac{p_f}{3N}\sum_i \Delta|F_i|^2 \qquad (19)$$

where ΔE and ΔF_i are the root mean squared error in the energy, forces, N is the number of atoms, the adjustable pre-factors p_ϵ starts with 0.02 and goes for 8 as the training ends; p_f from 1000 to 1. The starting learning rate is 0.001 and as training going, it decays with decay rate 0.95 and decay steps 20000. Optimization of loss function is done using the Adam stochastic gradient descent method. Training data consists of energies and forces from two AIMD simulations for neat-water and cavity-water systems. The batch-size is 4. The training process goes for 4,000,000 steps. The two AIMD simulations generate 120,000 frames and we build 20 data sets to train. After the model is sufficiently trained, model parameters can be frozen for use in MD simulations. We trained the two systems to obtain a more accurate model for water molecule behavior near the cavity interface and in the bulk liquid phase.

Recent development of DPMD package provides a module to train a DNN for estimation of the four Wannier center (WC) coordinates (with respective to oxygen atom).[25] Basing on it, we develop modules to train DNN for direct prediction of both the 3 dipole components P_x, P_y, P_z and 6 primitive quadrupole components $Q_{xx}, Q_{xy}, Q_{xz}, Q_{yy}, Q_{yz}$. The training process for each moment goes for 2,000,000 steps with a batch step of 5. All the other parameters are the same as that of the DNN for potential energy.

Classical Simulation Setup

DPMD-kit provides LAMMPS support through a third-party package to produce classical MD simulations using the frozen DNN models to compute the atomic interactions. In this way, large time-scale simulations are accessible at the quantum accuracy. We run NVT simulations in LAMMPS for systems of 64, 128, 256 waters with a cavity of radius 4.1 Å at the center. We apply the Nosé-Hoover thermostat chain of length 3 to maintain a temperature of 330 K. The system size $L = (\frac{N}{\rho} + \frac{4\pi}{3}r_c^3)^{\frac{1}{3}}$, where N is water number, number density $\rho = 33.3285$ (nm)$^{-3}$ (or 0.997 g/cm^3),r$_c$ = 4.1 Å . The DPMD simulation runs for 1500 ps, where the first 500 ps for equilibration and 1000 ps for data production. The time step is 0.5 fs and trajectory is recorded every 0.01 ps (20 steps).

Results and Discussion

We first list the dipole and quadrupole moments to compare with experimental values and previous reports. Next we display that the DPMD with good accuracy reproduces the distributions of moment elements in comparison with that are determined by AIMD. Last we show that the DPMD gives reasonable agreement with the local potential through multipole contributions from the AIMD calculations, allowing for the 3rd-cumulant term calculation over 6 ns through the DPMD.

Listed in Table 1 are the moment properties for both water monomer and water molecule in the liquid phase. In accord with the previous calculations, we report moment properties in the water molecular local coordinate system with the center of mass (COM) as the origin. As for the monomer in the box with L=12.4295 Å , the oxygen atom O position is at (2.9340,2.0000,3.0000), the first hydrogen H$_1$ at (3.5292,1.2320,3.0000) and the second hydrogen H$_2$ at (3.5292,2.7680,3.0000). As for the monomer local coordinate system, $\mathbf{e}_x$ is the interior bisector of the angle H$_1$-O-H$_2$; the norm direction of the water molecular plane $\mathbf{e}_z$ = $\mathbf{OH_1} \times \mathbf{OH_2}$; $\mathbf{e}_y = \mathbf{e}_z \times \mathbf{e}_x$. Correspondingly, the atomic dipole moment contributes 3.16 D,

and the 8 valence electrons contribute -1.32 D to the total dipole moment 1.84 D, which is in agreement with value 1.86 D from both MP2 calculation[30] and experimental observation.[31] The DFT theory with BLYP functional in box of L = 10.6 Å in the work by Silvestrelli[16] gives 1.87 D. Roland reported the finite-size effect[18] that the dipole moments decreases from 1.87 to 1.81 D as the box size L increases from 10.58 Å to infinite. Analogously, when we calculate in a larger box L = 16.00 Å , we obtain a smaller dipole moment 1.82 D. In the liquid phase, the average water dipole moment over 60,000 configurations of 64 waters is 2.72 D, in agreement with the value 2.70 D estimated by combining far-IR vibration-rotation-tunneling spectroscopy and *ab initio* calculation up to the largest cluster limit. It was reported[16] that for 64 waters system, the average value over 12 configurations from AIMD on DFT level is 2.95 D. The distribution was broad with a peak at 2.80 D. However both the average value and maximum value is within our first-sigma confidence interval.

For the monomer water, our eigenvalues of traceless quadrupole moment are in good agreement with both previous DFT calculation[17] -0.13, 2.58, -2.45 D·Å and experiment values (shown in the parentheses in Table 1).[32] For the water molecule in liquid phase, our average eigenvalues over 360 configurations are close to the previous calculations -0.22, 3.38, -3.16 D·Å by DFT over 12 configurations. Having established that our calculation is satisfactory in comparison with previous work and experiments, we are confident to display how the water molecule is polarized by the surrounding molecules in the liquid phase. To this end we give the three diagonal elements of primitive quadrupole Q in the local frame, because in the lab frame all of them would exhibit the similar distribution as well as close average values due to the thermodynamic averaging process. The dipole e_x element increases by 46.7% when water molecule goes into the liquid phase. This is attributed primarily to the significant compression of the valence electron cloud in this direction by the surrounding molecules, since the average length of O-H bond increases slightly by 2.0% (0.02Å) and average H-O-H angle by 0.8% as reported.[16] The less negative average Q_{xx} and Q_{yy} of water in the liquid also suggest that of the neighboring molecule compress each other in the these

two directions, while the more negative Q_{zz} indicates that electron cloud is stretched in the normal direction.

Table 1: Electrostatic dipole moment $\mathbf{P}$ of water molecule in unit of Debye (D), three eigenvalues of traceless quadrupole moment Q' in D·Å and three diagonal element of primitive quadrupole moment Q. The experimental values are shown in parentheses. The eigenvalues are in local frame with center of mass as origin. As for the primitive diagonal elements, the local coordinate system origin is on oxygen atom.

		$\mathbf{e}_x$	$\mathbf{e}_y$	$\mathbf{e}_z$
Monomer	$\mathbf{P}$	1.84 (1.85)	0.00	0.00
Liquid	$\mathbf{P}$	2.70	0.00	0.00
Monomer	Q'	-0.13 (-0.13)	2.56 (2.63)	-2.43 (-2.50)
Liquid	Q'	-0.15	3.13	-2.98
Monomer	Q	-3.00	-3.76	-2.10
Liquid	Q	-2.83	-1.92	-3.95

Having calculated the dipole and quadrupole moments with good accuracy, we feed the DNN with these data to train models for potential and moments. In the DPMD framework, the accuracy is quantified in terms of the root-mean-square error, and our potential model gives energy accuracy with 0.3 meV and forces with 56 meV/Å ; our moments model gives dipole with 0.04 D and primitive quadrupole with 0.01 D·Å . As shown in Fig.1, the excellent agreements of atomic radius distribution function (RDF) between DPMD and AIMD trajectories suggest that DPMD reproduces the trajectories sufficiently. Also, the diffusion constant D of neat water system, is found to be 0.539 Å^2/ps in the AIMD and 0.512Å^2/ps for the DPMD trajectory, showing the dynamics is modeled as well. Particularly, the oxygen-center RDF indicates that the we can approach a bulk-like region at a distance of 9.9 Å away from the center of cavity of radius 4.1 Å . Consequently, it suggests that it need 256 waters (at least) to provide us a good zero-reference for electrostatic potential calculations.

To assess the moments agreement between DPMD and AIMD, we plot the distributions of dipole moment in Fig.2 and that of quadrupole moment in Fig.3. Note that since the moment distributions in the lab frame should be of no significant difference, we display the distributions of moment in the local coordinate system established as mentioned above
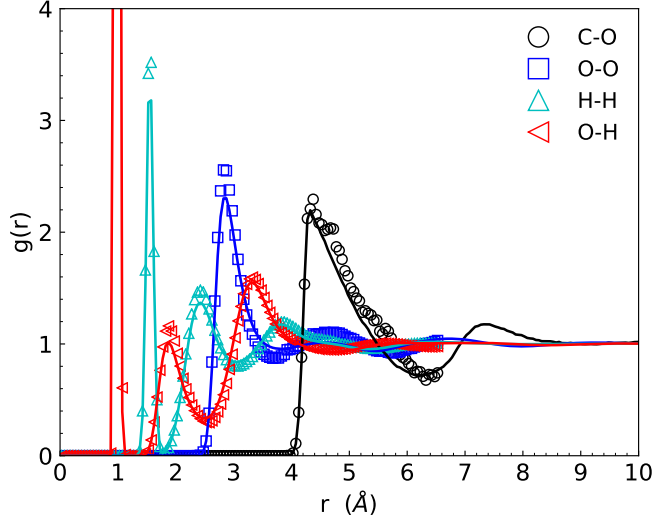
Figure 1: Radius distribution function (RDF) from AIMD and DPMD simulations. The circle symbols are for the RDF of oxygen atom referenced to cavity center from DFT 30 ps simulation. The squares are for the DFT oxygen-oxygen, up-triangles for the DFT hydrogen-hydrogen and left-triangles for the DFT oxygen-hydrogen. The solid lines are for the 256 water system from the DPMD (1000 ps) for 64 water system

for monomer water. Since it is the origin of the local coordinate system, the oxygen atom contributes nothing to moments. As displayed, the distributions are well approximately Gaussian. Dipole moment distributions show that the average water dipole moment is almost along the interior bisector of the H1-O-H2 angle. As for the primitive quadrupole, the average values of off-diagonal elements are zero. The most negative Q_{zz} is attributed to the lone pair orbitals. The excellent agreement for both dipole moments and primitve quadrupole element calculations between AIMD and DPMD allows us to explore the local potential contribution to the ion hydration free energy. Applying DPMD simulation over several nano-seconds makes us assess a convergent 3rd cumulant term with *ab initio* accuracy.

In table 2, We list the dipole moment contribution $\delta\phi_D$, non-symmetrical primitive moment contribution $\delta\phi_{Q2}$ and symmetrical primitive moment contribution $\delta\phi_{Q1}$ for different systems. Comparison of results from AIMD and DPMD suggests that with reasonable agreement DPMD reproduce the $\delta\phi_D$ and $\delta\phi_{Q2}$ contributions. And it is shown that these two contributions get convergent within the first hydration shell ($r \leq 6.5$Å). The sum of two

13

short-range contributions by DPMD is -0.39 V. As for the net potential, the Bethe potential contributions cancels out exactly when the ion go across two interfaces from vapor phase to the cavity center. The dipole contribution to the surface potential ϕ_{sp} is 0.48 V (referenced to the vapor phase) reported in the previous DFT work.[15] Therefore the center potential $\langle \phi \rangle_{M_\lambda} = 0.09$ V , which is close to the estimation 0.08 V in that work.[15] However these result is only from the first cumulant term as mentioned in the theoretical section.

As shown in Fig. 4, the potential increment of DPMD agrees well with that of AIMD and in the bulk-like region of the system with 256 waters where distant r > 9.9 Å , the average Bethe potential is 3.48 V. This is a little off the 3.63 V in the neat water system and previous report of 3.84 V[15] and of 3.50 V[10] . The difference of Bethe potential is primarily attributed to the different water number density, since Bethe potential is proportional to the water number density ρ. Having calculated the stable center potential $\langle \phi \rangle_{M_\lambda}$, the third cumulant term contribution $\frac{q^2}{6(kT)^2} \langle \delta\phi^3 \rangle_{M_\lambda}$ to the local potential is +0.22 V obtained from simulations totally over 6 ns, and thus the local potential $\phi_{lp} = -3.87 + 0.22 = -3.65$ V

Table 2: Dipole moment contribution $\delta\phi_D$ and non-symmetric quadrupole moments contribution $\delta\phi_{Q2}$ and Bethe potential contribution $\delta\phi_{Q1}$ the center potential $\langle \phi \rangle_{M_\lambda}$. The last column is the 3rd cumulant contribution to the local potential ϕ_{lp}. The r_{max} is the upper limit of the cumulative sum of dipole and quadrupole contributions, for which the bin size is 0.1 Å .

System	running time (ps)	r_{max} (Å)	$\delta\phi_D(V)$	$\delta\phi_{Q2}(V)$	$\delta\phi_{Q1}(V)$	3rd cumulant (V)
DFT 64	30	6.50	-0.22	-0.14		
DPMD 64	1000	6.50	0.24	0.15		
DPMD 128	1000	8.00	0.23	0.16		
DPMD 256	1000	9.90	0.23	0.16	3.48	-0.31
DPMD 256	6000	9.90	0.22	0.16	3.48	-0.22

Conclusion

First, Beyond the limits of both size and time scale of previous calculations by AIMD, the water molecular dipole and quadrupole moments in the water local coordinate are calculated,
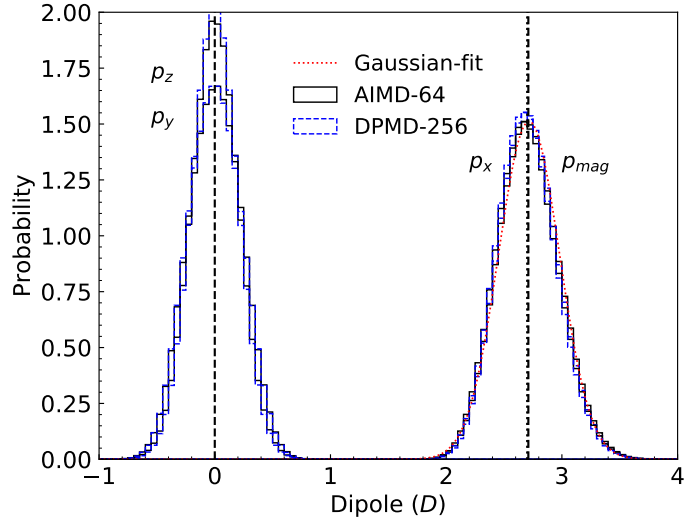
Figure 2: The distributions of water molecular dipole moment magnitude and three elements in the water molecular local frame. The solid lines are from DFT 30 ps simulation of 64 waters; the dashed lines are from DPMD 1000 ps simulation of 256 water system. The vertical dashed lines are the mean values from DFT simulation, and for the magnitude p_m, with standard deviation in parentheses, is of 2.72(0.26) D, for the p_x of 2.70(0.26) D; p_y of 0.00(0.20) D; p_z of 0.00(0.23)D.The red dotted line is the Gaussian distribution with same mean(sigma) as that of magnitude distribution from AIMD.
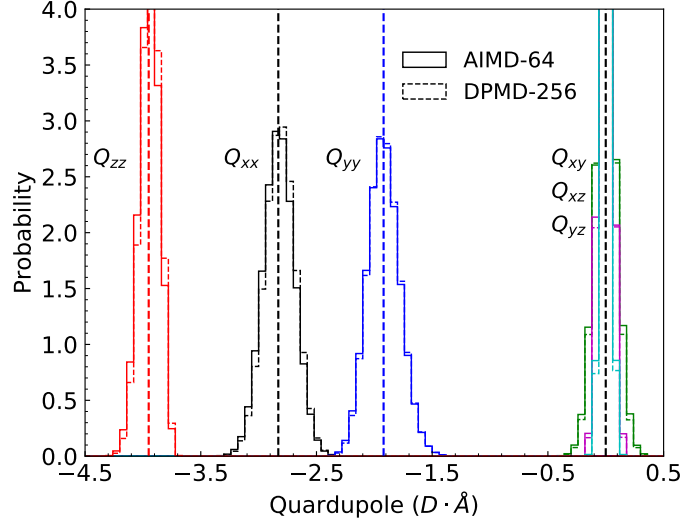
Figure 3: The distributions of water molecular quadrupole moment elements in the water molecular local frame. The solid lines are from DFT 30 ps simulation of 64 waters; the dashed lines are from DPMD 1000 ps simulation of 256 waters. The mean value and standard deviation (in the parenthese) from the DFT simulation, and for the Q_{xx} are of -2.83(0.14) $D{\cdot}\text{Å}$, the Q_{yy} of -1.92(0.14) $D{\cdot}\text{Å}$, the Q_{zz} of -3.95(0.09) $D{\cdot}\text{Å}$, the Q_{xy} of -0.00(0.10) $D{\cdot}\text{Å}$, Q_{xz} of 0.00(0.05) $D{\cdot}\text{Å}$ and Q_{yz} of 0.00(0.04)$D{\cdot}\text{Å}$.
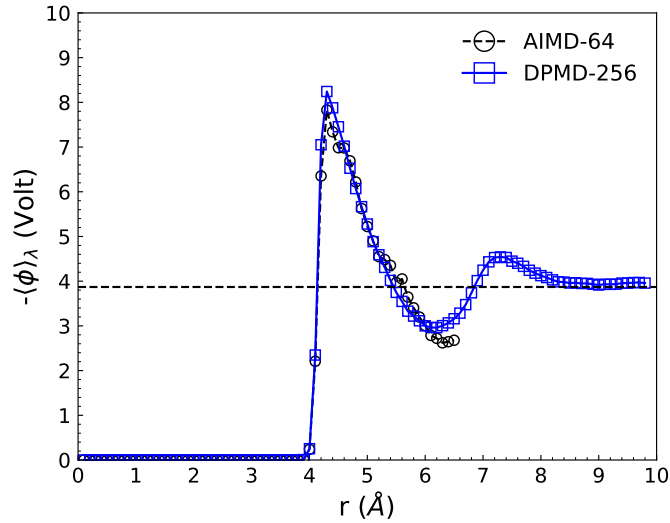

Figure 4: Cavity center potential $-\langle\phi\rangle_{M_\lambda} = \delta\phi_D + \delta\phi_{Q1} + \delta\phi_{Q2}$ as function of distance to the center. The open circles are from DFT 30 ps simulation of 64 waters; the open squares are from DPMD 1000 ps simulation of 256 waters, which $\delta\phi$ is convergent to 3.87 Volt at distance of 9.9 Å .

16

unraveling how the water molecule is polarized in the liquid phase. It is that the valence electron cloud are stretched along the norm direction of the water molecular plane, and are compressed in the other two orthogonal directions. Second, the Deep Neural Network models reproduce moments with a good accuracy, indicating that it is a powerful tool to approach the environment dependence of the multipole moment, allowing us to compute electrostatic potential that play a crucial in chemical process at low cost and with AIMD accuracy. Third, as an illustration of the possible applications, we calculate the local potential contribution to the ion hydration free. As high as the 3rd cumulant term we get a potential scale as -3.85 V. This result would be more robust and insightful if we go for larger system to include a vapor-water surface so that we can obtain and compare the net potential with the experimental scale -0.40 V derived from ion hydration data.

References

(1) Pollard, T.; Beck, T. L. Quasichemical Analysis of the Cluster Pair Approximation for the Thermodynamics of Proton Hydration. *J. Chem. Phys.* **2014**, *140*, 224507.

(2) Pollard, T. P.; Beck, T. L. The Thermodynamics of Proton Hydration and the Electrochemical Surface Potential of Water. *J. Chem. Phys.* **2014**, *141*, 18C512.

(3) Pollard, T. P.; Beck, T. L. Toward a Quantitative Theory of Hofmeister Phenomena: From Quantum Effects to Thermodynamics. *Curr. Opin. Colloid Interface Sci.* **2016**, *23*, 110–118.

(4) Halliwell, H. F.; Nyburg, S. C. Enthalpy of hydration of the proton. *Trans. Faraday Soc.* **1963**, *59*, 1126–1140.

(5) Y.Marcus, *Ion Solvation*; John Wiley: New York, 1985.

(6) Ashbaugh, H. S.; Asthagiri, D. Single ion hydration free energies: A consistent compar-

ison between experiment and classical molecular simulation. *The Journal of Chemical Physics* **2008**, *129*, 204501.

(7) Latimer, W. M.; Pitzer, K. S.; Slansky, C. M. The Free Energy of Hydration of Gaseous Ions, and the Absolute Potential of the Normal Calomel Electrode. *The Journal of Chemical Physics* **1939**, *7*, 108–111.

(8) Tissandier, M. D.; Cowen, K. A.; Feng, W. Y.; Gundlach, E.; Cohen, M. H.; Earhart, A. D.; Coe, J. V.; Tuttle, T. R. The Proton's Absolute Aqueous Enthalpy and Gibbs Free Energy of Solvation from Cluster-Ion Solvation Data. *The Journal of Physical Chemistry A* **1998**, *102*, 7787–7794.

(9) Kathmann, S. M.; Kuo, I.-F. W.; Mundy, C. J.; Schenter, G. K. Understanding the Surface Potential of Water. *The Journal of Physical Chemistry B* **2011**, *115*, 4369–4377, PMID: 21449605.

(10) Leung, K. Surface Potential at the AirWater Interface Computed Using Density Functional Theory. *The Journal of Physical Chemistry Letters* **2010**, *1*, 496–499.

(11) Beck, T. L.; Paulaitis, M. E.; Pratt, L. R. *The Potential Distribution Theorem and Models of Molecular Solutions*; Cambridge University Press, 2006.

(12) Shi, Y.; Beck, T. L. Length scales and interfacial potentials in ion hydration. *The Journal of Chemical Physics* **2013**, *139*, 044504.

(13) Wilson, M. A.; Pohorille, A.; Pratt, L. R. Comment on "Study on the liquid–vapor interface of water. I. Simulation results of thermodynamic properties and orientational structure". *The Journal of Chemical Physics* **1989**, *90*, 5211–5213.

(14) Doyle, C. C.; Shi, Y.; Beck, T. L. The Importance of the Water Molecular Quadrupole for Estimating Interfacial Potential Shifts Acting on Ions Near the Liquid–Vapor Interface. *The Journal of Physical Chemistry B* **2019**, *123*, 3348–3358, PMID: 30920221.

(15) Remsing, R. C.; Baer, M. D.; Schenter, G. K.; Mundy, C. J.; Weeks, J. D. The Role of Broken Symmetry in Solvation of a Spherical Cavity in Classical and Quantum Water Models. *The Journal of Physical Chemistry Letters* **2014**, *5*, 2767–2774, PMID: 26278076.

(16) Silvestrelli, P. L.; Parrinello, M. Water Molecule Dipole in the Gas and in the Liquid Phase. *Phys. Rev. Lett.* **1999**, *82*, 3308–3311.

(17) Silvestrelli, P. L.; Parrinello, M. Structural, electronic, and bonding properties of liquid water from first principles. *The Journal of Chemical Physics* **1999**, *111*, 3572–3580.

(18) Sagui, C.; Pomorski, P.; Darden, T. A.; Roland, C. Ab initio calculation of electrostatic multipoles with Wannier functions for large-scale biomolecular simulations. *The Journal of Chemical Physics* **2004**, *120*, 4530–4544.

(19) Behler, J. First principles neural network potentials for reactive simulations of large molecular and condensed systems. *Angewandte Chemie International Edition* **2017**, *56*, 12828–12840.

(20) Chmiela, S.; Tkatchenko, A.; Sauceda, H. E.; Poltavsky, I.; Schütt, K. T.; Müller, K.-R. Machine learning of accurate energy-conserving molecular force fields. *Science advances* **2017**, *3*, e1603015.

(21) Zhang, L.; Han, J.; Wang, H.; Car, R.; Weinan, E. Deep potential molecular dynamics: a scalable model with the accuracy of quantum mechanics. *Physical review letters* **2018**, *120*, 143001.

(22) Wang, H.; Zhang, L.; Han, J.; Weinan, E. DeePMD-kit: A deep learning package for many-body potential energy representation and molecular dynamics. *Computer Physics Communications* **2018**, *228*, 178–184.

(23) Bonati, L.; Parrinello, M. Silicon liquid structure and crystal nucleation from ab initio deep metadynamics. *Physical review letters* **2018**, *121*, 265701.

(24) Cheng, B.; Engel, E. A.; Behler, J.; Dellago, C.; Ceriotti, M. Ab initio thermodynamics of liquid and solid water. *Proceedings of the National Academy of Sciences* **2019**, *116*, 1110–1115.

(25) Zhang, L.; Chen, M.; Wu, X.; Wang, H.; Car, R., et al. Deep neural network for Wannier function centers. *arXiv preprint arXiv:1906.11434* **2019**,

(26) Wolfgang Schmickler, E. S. *Interfacial Electrochemistry*; Oxford University Press: Oxford, 1996.

(27) Fawcett, W. R. *Liquid, Solutions, and Interfaces: from Classical Macroscopic Descriptions to Modern Microscopic Details*; Oxford: New York, 2004.

(28) Hummer, G.; Pratt, L. R.; García, A. E. Free Energy of Ionic Hydration. *The Journal of Physical Chemistry* **1996**, *100*, 1206–1215.

(29) Horváth, L.; Beu, T.; Manghi, M.; Palmeri, J. The vapor-liquid interface potential of (multi)polar fluids and its influence on ion solvation. *The Journal of Chemical Physics* **2013**, *138*, 154702.

(30) Batista, E. R.; Xantheas, S. S.; Jónsson, H. Molecular multipole moments of water molecules in ice Ih. *The Journal of Chemical Physics* **1998**, *109*, 4546–4551.

(31) Clough, S. A.; Beers, Y.; Klein, G. P.; Rothman, L. S. Dipole moment of water from Stark measurements of H2O, HDO, and D2O. *The Journal of Chemical Physics* **1973**, *59*, 2254–2259.

(32) Verhoeven, J.; Dymanus, A. Magnetic Properties and Molecular Quadrupole Tensor of the Water Molecule by Beam-Maser Zeeman Spectroscopy. *The Journal of Chemical Physics* **1970**, *52*, 3222–3233.